

PCCP

Accepted Manuscript



This is an *Accepted Manuscript*, which has been through the Royal Society of Chemistry peer review process and has been accepted for publication.

Accepted Manuscripts are published online shortly after acceptance, before technical editing, formatting and proof reading. Using this free service, authors can make their results available to the community, in citable form, before we publish the edited article. We will replace this *Accepted Manuscript* with the edited and formatted *Advance Article* as soon as it is available.

You can find more information about *Accepted Manuscripts* in the [Information for Authors](#).

Please note that technical editing may introduce minor changes to the text and/or graphics, which may alter content. The journal's standard [Terms & Conditions](#) and the [Ethical guidelines](#) still apply. In no event shall the Royal Society of Chemistry be held responsible for any errors or omissions in this *Accepted Manuscript* or any consequences arising from the use of any information it contains.

Boron-nitride nanotube triggered self-assembly of hexagonal boron-nitride nanostructure

Yunfang Li *

College of Mechanical Engineering, Linyi University, Linyi, Shandong 276005, People's Republic of China. E-mail: liyunfang@lyu.edu.cn

Molecular mechanics results show that hexagonal boron nitride (*h*-BN) membrane can spontaneously assemble on the single-walled boron nitride nanotube (BNNT) in a scroll or helical manner, showing an interesting dependence on *h*-BN width. The size of BNNTs should meet the required conditions to guarantee the self-assembly. Further analyses of energy components and structural geometry show that this unique phenomenon is the result of the combined action of the van der Waals interaction and the π - π stacking effect. The *h*-BNs with arbitrary sizes and shapes can wrap onto BNNTs to form various configurations. The self-assembly conditions and the stability of the formed nanoconfigurations are investigated for numerous potential applications.

1. Introduction

Ground-breaking experiments of graphene have activated a revolution in the characterization and potential applications of two-dimensional materials.^{1,2} Hexagonal boron nitride (*h*-BN) is a one-atom-thick material that analogous to graphene because it is isoelectronic and isomorphic to the graphene honeycomb lattice.³ However, thin *h*-BN membranes are fundamentally different from graphene, possessing large band gap,⁴⁻⁶ higher chemical and thermal stability,^{7,8} and exceptional hardness,^{9,10} making it potential

candidate for use as insulators in memory diodes,⁷ high-temperature lubricants,^{7,8} or electrocatalysts.¹¹

Experimental and theoretical studies have validated that under the help of metallic nanowire, carbon nanotube or water, highly elastic graphene can overcome energy barrier and self-assemble on them into variety of other three-dimensional nanostructures.¹²⁻¹⁷ This unique behavior arouses one intensively to imagine whether the similar structured *h*-BN sheets have such self-assembly properties as well. With selective and strong van der Waals (vdW) coupling to planar *h*-BN surfaces,^{18,19} highly rigid boron-nitride nanotubes (BNNTs) may be the most appropriate substrates for *h*-BN sheets to adhere and self-assemble. It is well known that the unique properties and applications of two-dimensional materials mainly depend on their flat monoatomic membrane sheet structures. The *h*-BN with high flexibility can deform and self-assemble on nanotube to form other distinct new nanostructures, which may extends many additional fascinating phenomena and important applications of the *h*-BN. Furthermore, novel composite functional materials could be prepared if planar *h*-BN nanostructures of various shapes and sizes are self-assembled on the surfaces of nanoscale materials. It is urgent to give a direct atomic-level picture of the interaction mode and geometrical structures between two-dimensional *h*-BN sheets and one-dimensional BNNTs, which may inspires enormous interests in theoretical and experimental studies to explore new structure and property of *h*-BN. Great effect can be shortly sparked on the synthesis of novel *h*-BN-based functional nanomaterials and eventually on their applications into more extensive nanodevices.

In the present study, convincing theoretical results are presented to reveal how the

h-BN sheet interacts with the BNNT and what is the shape of the *h*-BN adhering onto the sidewall of the tubes. In particular, the possible interacting mechanism is examined and the analytical model is proposed to establish the nature of the interaction of *h*-BN sheet with the BNNT. This study is not only helpful for the better understanding of the stability and properties of *h*-BN at an atomistic level, but also essential to deepen the insight into the stability of two-dimensional materials. Furthermore, it can help guide exploring new theories, providing theoretical supports for related practical experiments and eventually beneficial for fabricating functional nanodevices.

2. Method

The self-assembly of *h*-BN nanostructures on BNNTs was simulated by molecular mechanics simulations under the constant volume and constant temperature dynamics (NVT) ensemble. The atomic interactions were described by the Universal forcefield (UFF), which provides a general approach to molecular mechanics for molecules and materials composed of elements throughout the periodic table. UFF has been carefully validated for predicting geometries and conformational energy differences of main-group compounds, metal complexes, and organic molecules. All the forcefield parameters include a set of hybridization, effective nuclear charges, and connectivity.²⁰⁻²¹ The UFF is well suited for dynamics simulations because it allows more accurate vibration measurements than many other forcefields, which do not distinguish bond strengths. Such a universal approach suffers the disadvantage of only providing moderate accuracy for any given system but possesses the corresponding advantage that it may be applied broadly. The UFF method is an excellent general purpose forcefield and empirical technique that optimizes structures with a high level of accuracy and at comparably little

computational expense. Implementations on this forcefield have been rigorously tested and results are in agreement with published works.^{22,23} The potential energy (E_P) of the UFF is expressed as the sum of the valence or bonded and nonbonded interactions:

$$E_P = E_R + E_\theta + E_\tau + E_\omega + E_{el}$$

The bonded interactions include the bond stretching E_R , angle bending E_θ , dihedral angle torsion E_τ , and inversion terms E_ω . The nonbonded interactions include the van der Waals interaction E_{vdw} and the electrostatic interaction E_{el} . The bond stretching is expressed as a harmonic term, the angle bending as a threeterm Fourier cosine expansion, and the torsion and inversion as cosine-Fourier expansion terms. The E_{vdw} is described by the 6-12 Lennard-Jones potential and the electrostatic term by the Coulomb interaction.^{20,21} The E_{vdw} is of fundamental importance to determine the scrolling dynamics. It is the component of the non-bond energy of the system, in kcal/mol. The E_{vdw} is calculated using a Lennard-Jones function and the parameters of E_{vdw} are obtained by fitting the measured experimental data of the cohesive energy and equilibrium density. In the systems of this work, the E_{vdw} describes the interaction between the h-BN and BNNT or between scrolled h-BN layers. During the calculation process, E_p and E_{vdw} will be calculated and recorded every 0.1 ps, and then the curves of E_p and E_{vdw} can be obtained.

The reliable Nose-Hoover-Langevin (NHL) dynamics in the thermostat was applied to control the temperature and generate the correct statistical ensemble. The simulations were carried out without periodic boundary conditions so that there is no pressure coupling. The velocity Verlet algorithm was adopted to integrate the equations of motion of the whole system. Here, the simulation for each case study was performed long enough to observe several cycles of thermal vibration. The interval of each MM simulation step

was typically 1.0 fs. All simulations were carried out at a constant temperature of 298 K. To enhance the quality of the calculations, the energy convergence and the force convergence tolerance were defined as 2×10^{-5} kcal/mol and 0.001 kcal/(mol.Å), respectively.

The *h*-BN sheets with various shape and BNNTs with different size and chirality were chosen to satisfy the simulations. The two ends of each BNNT were fixed rigidly with length of 1.23 Å to locate the position. Initially, *h*-BN nanostructures were located beside the BNNT vertically with a separation of about 5 Å in order to insure the distances between them within the range of the cutoff distance of vdW interaction. Thereafter, MM simulations were performed to investigate the self-assembly of *h*-BN sheets on BNNTs. During simulations, data were recorded every 0.1 ps to record the full-precision trajectory for further analysis.

3. Results and discussion

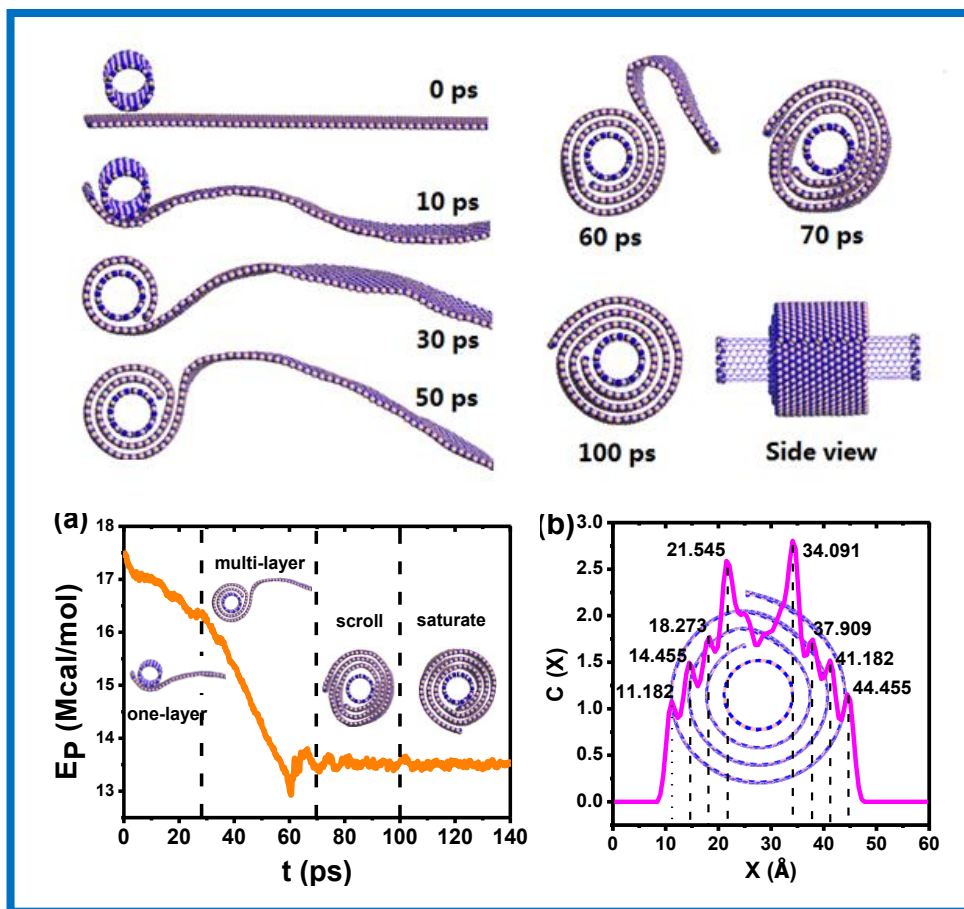


Fig. 1 Spontaneous scrolling of an *h*-BN sheet onto BNNT (10, 10). (a) E_p of the *h*-BN-BNNT system as a function of time. Insets are representative snapshots. (b) Concentration distribution profile of the final configurations in the X-direction.

The present work aims to reveal the self-assembly of *h*-BN on BNNTs and the corresponding properties at an atomic level. Fig. 1 shows how an *h*-BN membrane with size of $261.08 \times 28.87 \text{ \AA}^2$ rolls onto a (10, 10) BNNT with the diameter of 13.56 \AA and length of 66.41 \AA , with its two ends fixed. Initially, one tip of *h*-BN is positioned perpendicularly to the BNNT axis close to its surface. After be released, the *h*-BN resembles graphene to display discontinuous wrinkles or corrugations in several nanometers thick, showing its thermodynamic instability. At $t = 3 \text{ ps}$, the tip adheres

tightly onto the BNNT surface and fold with the core of tube, due to large vdW coupling. The vdW attraction acts as main driving force to make the *h*-BN moving forwards and scrolling onto BNNT continuously. At $t = 30$ ps, the *h*-BN just wraps the BNNT one circle with a tail, the sideview of which just like a tadpole. When $t = 50$ ps, the *h*-BN forms a double-layered scroll around the BNNT. Eventually, at $t = 70$ ps, *h*-BN forms a multiwalled scroll with the core of BNNT. But due to the high rolling speed, the scroll layers vibrate and equilibrate until about $t = 100$ ps (top and side views). However, the initial setup of the simulation may impact the self-assembly process and result. For example, when BNNT is placed near the middle of the *h*-BN, *h*-BN will wrap onto it to form knot instead of the coaxial-cable structure.

How the width of *h*-BN sheet affect the self-assembly process is further investigated. Fig. 2 provides the representative snapshots of an *h*-BN nanoribbon helically wrapping onto BNNT (10, 10). In Fig. 2a, the tip of the *h*-BN nanoribbon ($248 \times 11.362 \text{ \AA}^2$) is initially positioned on the BNNT vertically. The tip adheres onto BNNT fast ($t = 10$ ps) and then folds around BNNT in a spiral manner. The *h*-BN helix always has remarkably constant pitches and constant value 3.5 \AA of the gap between neighboring spirals during the wrapping process. Eventually, the *h*-BN forms a stable helical structure at $t = 80$ ps (side and top views). It is obviously that the width of *h*-BN also has great impact on the self-assembly of *h*-BN on BNNT. The spiral direction of the *h*-BN helix is determined by the initial deflection of the captured end of *h*-BN, which can be right-handed or left-handed with equal probability. It can be controlled by a small initial angle between the *h*-BN and the tube axis.

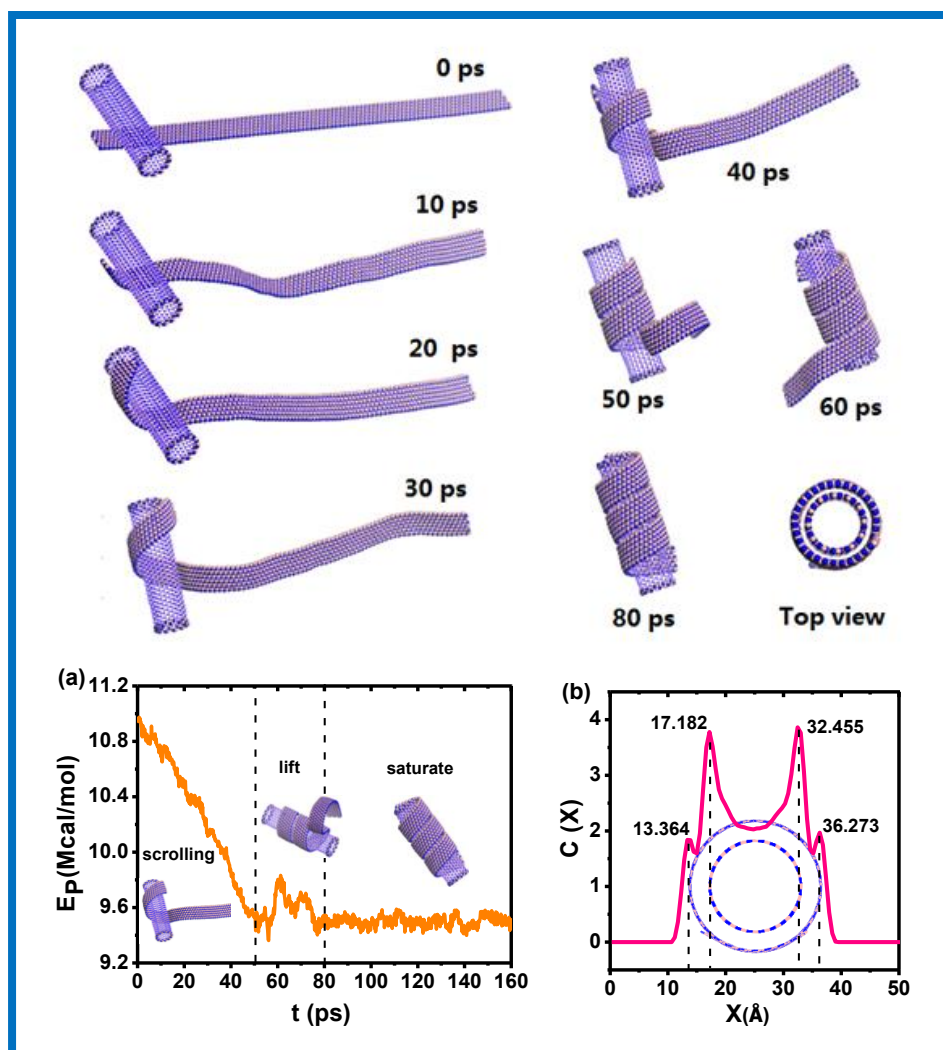


Fig. 2 Representative snapshots of an *h*-BN nanoribbon helically wrapping onto BNNT (10, 10). (a) E_P of the *h*-BN-BNNT system as a function of time. The insets are representative snapshots. (b) Concentration distribution profile of the final configuration in the X-direction.

To quantitatively reveal the energy evolution during the self-assembly, Figs. 1a and 2a plot the changes of E_P of the above-mentioned two systems against time respectively, the insets are representative snapshots. During the whole self-assembly courses, the E_P decrease with the increase of the contact area between *h*-BN and BNNT, which enhances

the stability of the system. Finally, E_p saturates, suggesting that systems reach the most stable states after h -BNs have fully self-assembled onto BNNT. The final geometric configurations of the self-assembled structures can be further characterized by the concentration distribution profile in the X-direction. The separation of the adjacent layers can be obtained by the distance between two neighboring peaks of the concentration profiles. From the peak details labeled in Figs. 1b and 2b, the distance of each gap is either 3.272 or 3.818 Å alternately due to the thermal vibration. When reaching full equilibrium, the average distance keeps a constant of 3.545 Å, which is very close to the wall thickness of the multiwalled BNNTs (3.4 Å).

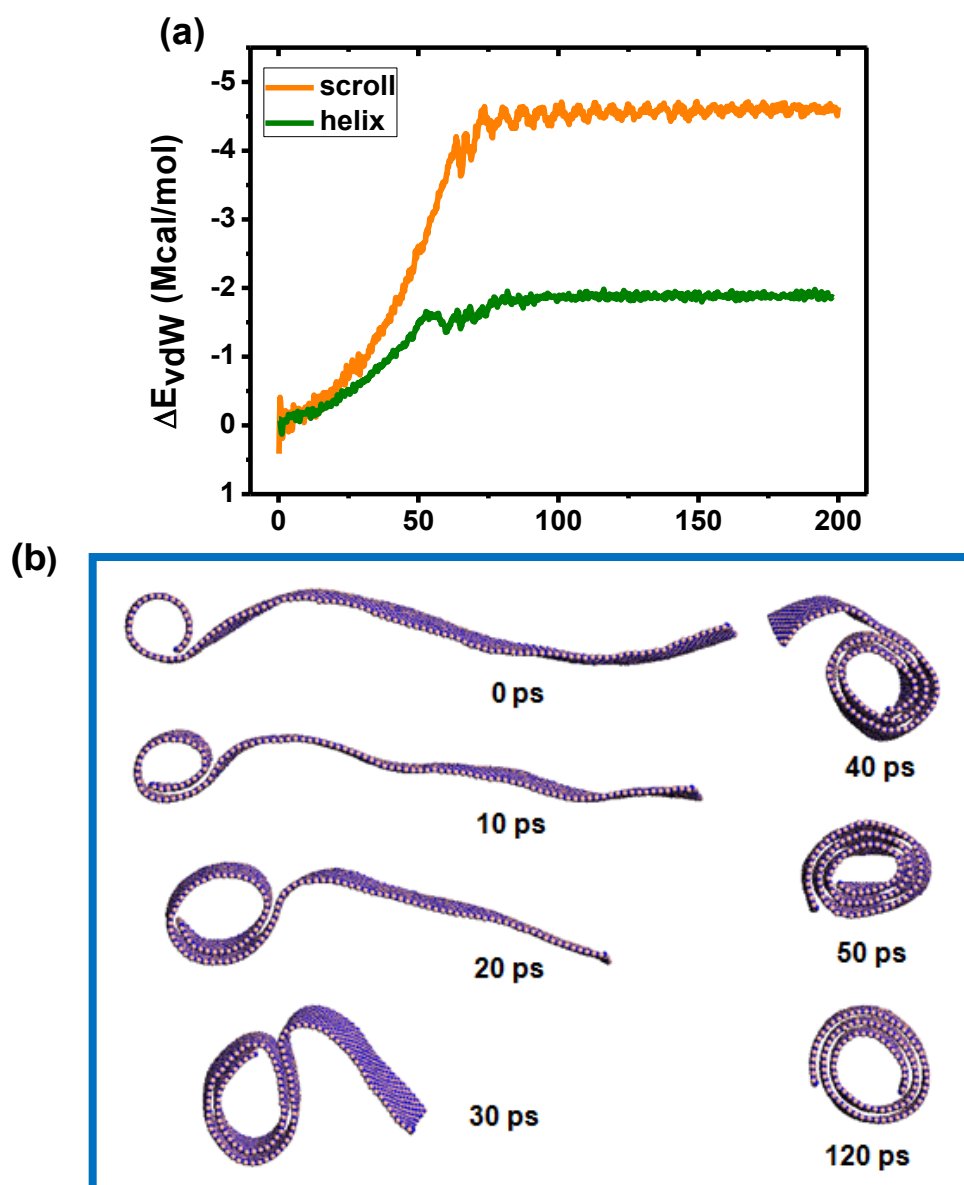


Fig. 3 (a) ΔE_{vdW} between *h*-BN and BNNT as a function of time in the scroll- and helix-forming processes. (b) Self-assembly of *h*-BN after remove the BNNT.

Such unique self-assembly is resulted from the combined action of the vdW interaction between the *h*-BN and BNNT and *h*-BN layers, as well as the offset face-to-face π - π stacking effect.^{24,25} The vdW interaction between the *h*-BN and BNNT

helps *h*-BN overcome the energy barrier that always tends to keep the *h*-BN GNS flat so that it may deform. After *h*-BN rolling the tube one lap, the vdW interaction between *h*-BN layers causes *h*-BN to form scroll configuration. The vdW interaction drives the *h*-BN continuously move toward the tube and undergoes self-assembly, which endows the *h*-BN with kinetic energy and sustains the self-assembly. The self-assembled speed is determined by the strength of vdW forces acting on the *h*-BN and the rate of its momentum dissipation, due to friction with the BNNT. As shown in Fig. 3a, the negative ΔE_{vdW} , indicating an attractive force, suggests that the vdW interaction between the *h*-BN and BNNT plays a dominant role in driving the continuous self-assembly of the *h*-BN and forming a scroll or helix depending on its size. Throughout the self-assembly courses, the vdW energy decreases significantly and finally reaches its minimum, which is nearly synchronous to the evolution of total potential energy E_p . The vdW energy has partially transformed to the internal energy for mechanical deformation of *h*-BN and partially converted into kinetic energy, thus sustaining the structural transition. As a result, the collapsed *h*-BNs have the largest area to contact, which reduces the systemic potential energy and enhances the stability of the *h*-BN-BNNT systems mostly.

The effect of the vdW interaction between *h*-BN layers in the scroll-forming process is further clarified. After the BNNT initials the *h*-BN to wrap it a coiling, the BNNT is removed to explore the afterward self-assembly of *h*-BN sheet. Just as shown in Fig. 3b, the tadpole-like *h*-BN is not collapse but self-scroll forward. The *h*-BN favours spontaneous scrolling once the sheet is curved to the extent that the edge makes sufficient contact with its inner surface. The vdW force between *h*-BN layers of the overlapped parts decreases the total free energy even though the curvature energy increased due to

bending. The *h*-BN rolls up continuously and the interior of the scroll is enlarging simultaneously ($t = 10 \sim 20$ ps). And at $t = 50$ ps, *h*-BN transforms into a scroll with a decrease in total free energy, and shrinks the hollow interior somewhat. The structure vibrates and eventually stables at $t = 120$ ps. This characteristic affirms the effect of the vdW interaction between *h*-BN layers in the scroll-forming process. The distance between the adjacent stacked layers is about 3.5 \AA , which is consistent with that of scroll formed on BNNT. Such a well-defined scroll facilitates the characterization of its physical properties and may have some new physical properties as compared with BNNT and *h*-BN.

Especially the offset face-to-face π - π stacking effect, an intermolecular interaction in the paralleled six-membered rings,^{24,25} stabilizes the adjacent paralleled *h*-BN layers to achieve the lowest energy of AB stack (side view of Fig. 1). It speculates that the π - π stacking interaction can provide two key elements for the self-assembly of *h*-BN; one is an energetic contribution that stems from the stacking itself, as such a contribution can thermodynamically drive the self-assembly process; and the other is specific directionality and orientation provided by the specific pattern of stacking.²⁶ The stacked *h*-BN layers should be exactly parallel and achieve the lowest energy of AB stack determined by the π - σ interaction, which is between the π electrons of one ring and the σ -framework around the inner edge of the cavity of the other ring above. Therefore, a parallel displaced π -stacking between *h*-BN and BNNT wall and *h*-BN layers should be the major organization of π - π interactions displacement, which causes *h*-BN to transform into scroll or helical construction adhering on the tube wall. The concentration distribution profiles show that the separations of each gap is 3.545 \AA , according well with

the parallel stacking distance of the π - π stacking interaction, further proving that the π - π stacking interaction plays a dominant role in the self-assembly process.

To realize the control to GNR helix, a key issue crucial to know is that the dependence of the diameter and chirality of BNNT in the self-assembly. From calculations, only when the diameter of BNNT (R) no smaller than 8.14 Å ($R \geq 8.14$ Å) that can induce the self-assembly of an h -BN. If the diameter of the BNNT is < 8.14 Å, the provided vdW interaction cannot help to overcome the energy barrier of h -BN, thus cannot induce the h -BN to wrap it. However, for slender h -BN nanoribbon with width of 11.362 Å, when the diameter of the BNNT is in the range from 8.41 to 9.49 Å, though h -BN can self-assemble, but forming knot instead of helix structure on it, because the curvature of the tube wall is so large that h -BN cannot bend to wrap helically, as shown the h -BN self-assembled on the armchair BNNT (6, 6). Only when R reaches to 9.49 Å can the h -BN nanoribbon produce a perfect helix outside the nanotube. The BNNT (7, 7) is the least armchair-shaped BNNT that can induce an h -BN sheet even with a very long length to completely wind onto the BNNT. Just as seen in Fig. 4a, the perfect h -BN helix can be formed on the surface of BNNTs with different chiralities when the diameter is larger than 9.49 Å.

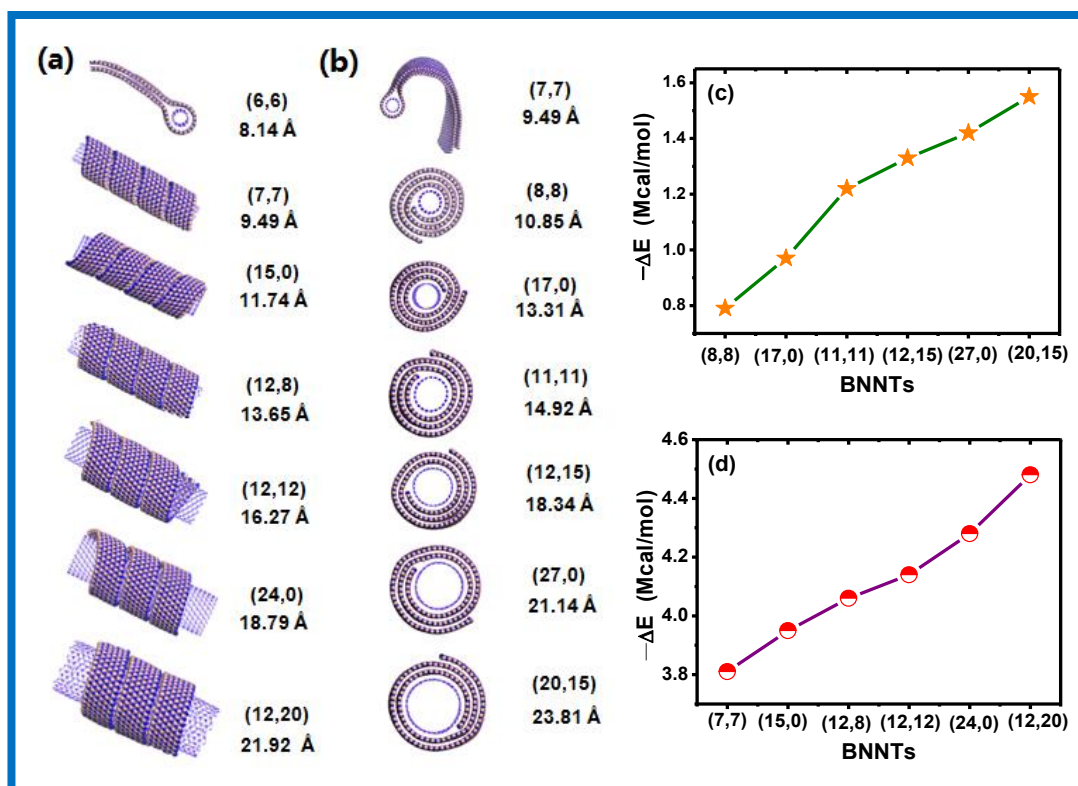


Fig. 4 The dependence of the diameter and chirality of BNNT in the self-assembly. (a) helical wrapping of a thin *h*-BN ribbon onto BNNTs with different diameter and chirality; (b) scrolling of a *h*-BN sheet onto BNNTs with different diameter and chirality; (c) ΔE between the *h*-BN helices and the different BNNTs; (d) ΔE between the *h*-BN scrolls and different BNNTs.

For relatively wider *h*-BN sheet with width of 28.87 Å, BNNTs with length 66.41 Å and diameter range from 8.41 to 10.85 Å can only induce *h*-BN sheet to form knot structure because of larger curvature of the tube wall, as shown the *h*-BN self-assembled on the armchair BNNT (7, 7). Only when $R \geq 10.85$ Å, *h*-BN can self-assemble on it and form perfect scroll, just as seen in Fig. 4b. Therefore, when the diameter of BNNT exceeds the critical value, the *h*-BN can scroll or wind onto any kinds of BNNTs

spontaneously and form scroll of helix sharp, indicating the self-assembly of *h*-BN is dependent strongly on the diameter and slightly on the chirality of BNNT.

To quantitatively clarify the influence of the chirality and diameter of BNNT, the adhesion energies of the assembled systems are calculated. It is well known that the potential energy difference is calculated as:²⁷

$$\Delta E = E_{\text{total}} - (E_{\text{BNNT}} + E_{h\text{-BN}}),$$

where E_{total} is the total potential energy of the self-assembled system, E_{BNNT} and $E_{h\text{-BN}}$ are the minimum energies of the isolated substances. When the assembled system achieves a minimum energy, the value of $(-\Delta E)$ can be defined as the adhesion energy of the two materials, as shown in Figs. 4c and d. Two curves show that the adhesion of the two materials depends strongly on the diameter and slightly on the chirality of BNNTs. The adhesion energy is increase with the increase of the tube diameter nearly linearly in helical and scrolled systems, proving the fact that the more flat of the BNNT wall (lower curvature) it is, the stronger adhesion intensity between *h*-BN and BNNT. It suggests that the *h*-BN helix and scroll on the BNNT with larger diameter is more stable. The formed nanoconfigurations are stable enough for numerous potential applications, because they can keep their shape no matter whether cooled or heated to any point of temperature.

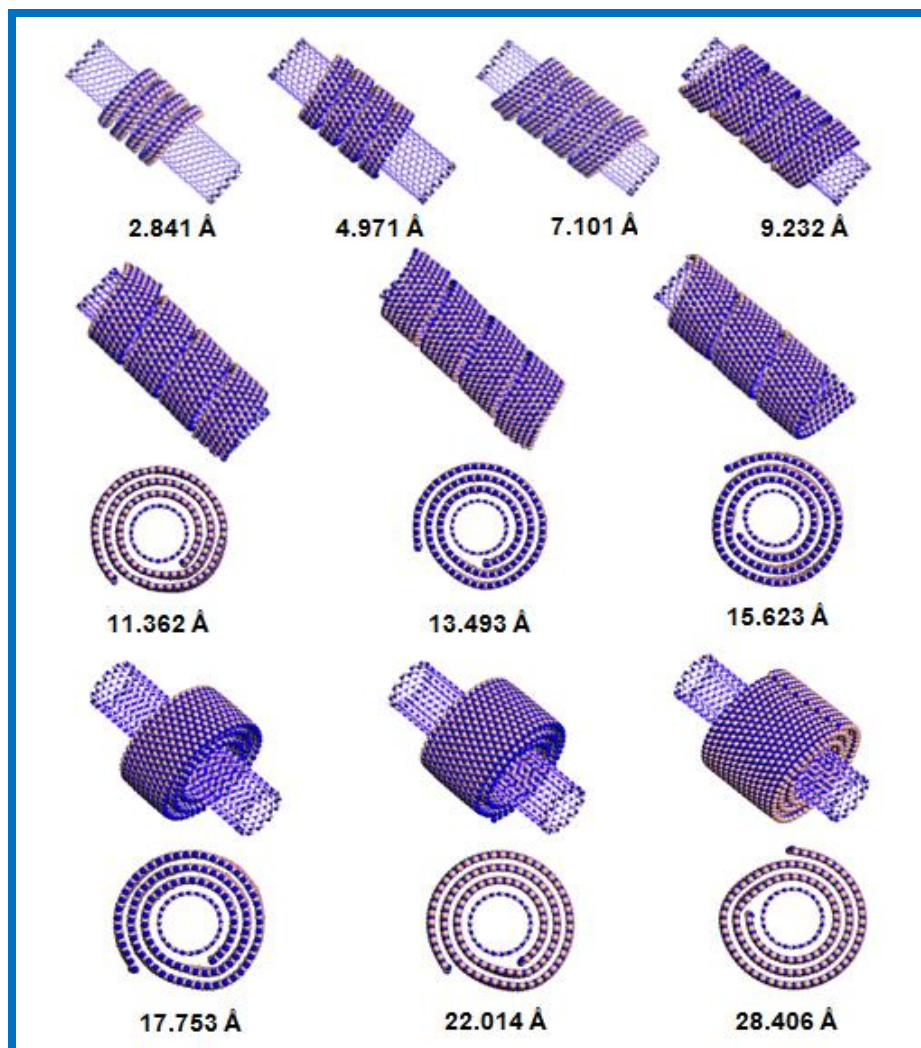


Fig. 5 The dependence of the *h*-BN width in the self-assembly. The insets are the width of *h*-BN.

The effect of the *h*-BN width (W) in the self-assembly is further studied, as shown in Fig. 5. The width of the narrowest *h*-BN is 2.841 Å, in which only contains one string of BN six-membered rings. Calculations show that, when $W \leq 9.232$ Å, thin *h*-BN ribbon can only form helix on BNNT surface. If the width is in the range $9.232 < W < 17.753$ Å, *h*-BN self-assembles on BNNTs can not only form helix but also scroll structures, leading to a mechanically bistable configuration, which is very different from graphene that a

graphene self-assembles on a carbon tube can only form a specific configuration. While when W larger than the threshold of 17.753 \AA ($W \geq 17.753 \text{ \AA}$), relative wider h -BN sheet can only form scroll. E_P of the systems as a function of time is tracked when an h -BN self-assembles on the BNNT to form helix and scroll from the same initial setup, respectively. The width of h -BN is 13.493 \AA , and the tube is long enough. Just as seen in Fig. 6, at the beginning, the variations of E_P are nearly the same. During the self-assembly, the decrease of the E_P in helix-forming process is quicker than that of scrolling-forming process. While when reach equilibrium, E_P of the scroll is lower than that of helix, indicating that scroll is more stable than helix.

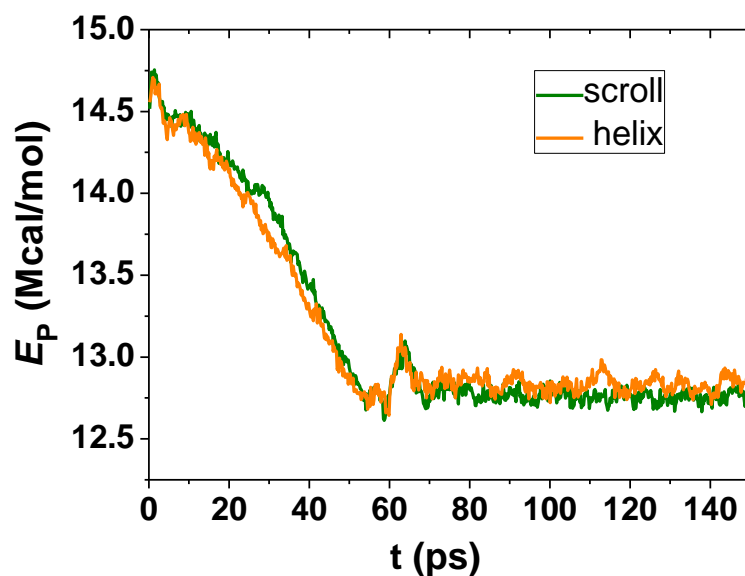


Fig. 6 E_P of the system as a function of simulation time when an h -BN self-assembles on the BNNT to form helix and scroll from the same initial setup, respectively.

A simple analytical model¹³ established by Patra. et al is explored to understand the conditions under which GNRs self-assemble into different structures outside BNNTs.

The total *h*-BN-BNNT coupling energy is described in the form as follows:

$$\begin{aligned}
 E_{total} &= E_{ela} + E_{T-S} + E_{S-S} \\
 E_{T-S} &= \sum_{i-tube, j-sheet} V_{i,j} = \langle E_{T-S} \rangle + E_{sym} \\
 E_{S-S} &= \sum_{i,j-sheet} V_{i,j}
 \end{aligned} \tag{1}$$

here, E_{ela} , E_{T-S} , and E_{S-S} are the intrinsic bending energy of *h*-BN sheets, the vdW binding energy between BNNTs and *h*-BN sheets, and the vdW energy for coupling of neighboring layers or edges of *h*-BN sheets, respectively. The i, j indices in the Lennard-Jones potential, $V_{i,j}$ run over atoms in the two subsystems. Thermodynamically, the occurrence of the self-assembly of an *h*-BN sheet on BNNT is determined by the competition between the *h*-BN-BNNT binding energy, E_{T-S} , and the *h*-BN intrinsic elastic bending energy, E_{ela} . When the energy barrier is overcome, the self-assembly of *h*-BN on BNNT is driven by the decrease of the E_{T-S} and E_{S-S} .

The elastic energy of the pristine *h*-BN is given by $E_{ela} = \sigma_{ela}A_{ela}$, where σ_{ela} is the strain energy density and A_{ela} is the total bending area.^{28,29} In the linear elastic regime, $\sigma_{ela} = D\kappa^2/2$, where $\kappa = (\kappa_1 + \kappa_2)/2$ is the local mean curvature and D is the flexural rigidity. The σ_{ela} is obtained by calculating the energy difference of unit area between the flat GNS and the folded cylinder. When a *h*-BN sheet folds on a BNNT, one of the two curvatures is $\kappa_{1(2)} \approx 0$. Therefore, the curvature is given by $\kappa = 1/R_{ela}$, where R_{ela} is the radius of the folded cylinder of *h*-BN sheet. Then the value of D can be calculated.

As shown in eq 1, the coupling energy, E_{T-S} , can be split into the ‘‘mean-field’’ term, $\langle E_{T-S} \rangle$, and the ‘‘symmetry-related’’ term, E_{sym} . The first term represents the vdW coupling between BNNT and *h*-BN sheet lattices that is averaged over the angle describing mutual orientation of the two subsystems (smearing of their hexagonal

lattices). The symmetry-related term accounts for the difference between the actual and smeared coupling (interferences) of the lattices in the BNNT and *h*-BN sheet structures.^{24,25} Due to the last term, the *h*-BN might have local potential energy minima for certain orientations with respect to the BNNT (symmetry locking).

The full BNNT and *h*-BN sheet coupling energy can be expressed as $E_{T-S} = -\sigma_{T-S}A_{T-S}$, where σ_{T-S} is the related (positive) energy density and A_{T-S} is the related coupling area. Analogously, the averaged and symmetry terms can be written as $\langle E_{T-S} \rangle = -\langle \sigma_{T-S} \rangle A_{T-S}$ and $E_{sym} = -\sigma_{sym}A_{T-S}$, respectively. The σ_{sym} can be estimated coefficient by placing an *h*-BN flake with a hexagonal shape on a large *h*-BN sheet.¹³ But compared with σ_{T-S} , σ_{sym} is very small and usually be ignored in this analytical model. Therefore, E_{T-S} can be easily obtained from the difference of the total vdW energy of the system at two different states, one state is the distance between GNS and Fe NW is in their normal binding length, the other one is the Fe NW is separated from the GNS by a very long distance.

The vdW coupling energy between *h*-BN sheet (in the case of sidewise coupling) is $E_{S-S} = -\sigma_{S-S}L_{S-S}$, where σ_{S-S} and L_{S-S} are the (positive) sidewise vdW binding energy density and the edge length of *h*-BN sheet, respectively. The sidewise vdW energy density between *h*-BN sheet, σ_{S-S} , is calculated as the difference of the (averaged) energies per unit area of two *h*-BN sheets placed in a plane with AB stack with separation 3.5 Å (optimization) and a long distance exceeding 100 Å (both fixed). Their armchair structures are facing each other without any sidewise shifting. From MM simulations, it calculated that $D \approx 48.612$ kcal/mol, $\sigma_{ela} \approx 0.230$ kcal/(mol Å²), and $\sigma_{S-S} \approx 0.734$ kcal/(mol Å²). However, σ_{T-S} is not constant, which will increase with the increase of BNNT diameters. When the diameter of BNNT towards infinity, the σ_{T-S} will increase

and infinitely close to the value of $0.734 \text{ kcal}/(\text{mol} \cdot \text{\AA}^2)$ that between planar *h*-BN layers. For example, between *h*-BN and BNNT (10,10), the $\sigma_{T-S} \approx 0.668 \text{ kcal}/(\text{mol} \cdot \text{\AA}^2)$. That why the scroll is more stable than helix configuration for a *h*-BN. Compared these values of D and σ_{ela} with that of graphene ($D \approx 27.9 \text{ kcal}/\text{mol}$, $\sigma_S \approx 0.102 \text{ kcal}/(\text{mol} \cdot \text{\AA}^2)$), concluding that the structural stability and mechanical properties of *h*-BN are superior to graphene.

The necessary energy condition for the realization of the BNNT-activated self-assembly of *h*-BNs is that the total energy in the self-assembled state is smaller than at the beginning:

$$E_{total} < 0 \quad (E_{T-S} + E_{S-S} < -E_{ela}).$$

During the self-assembly, the E_{T-S} and E_{S-S} drop rapidly in every infinitesimal distortion of the system along the self-assembly trajectory due to the increase of the A_{T-S} and A_{S-S} , and therefore, the self-assembled system will become more and more stable.

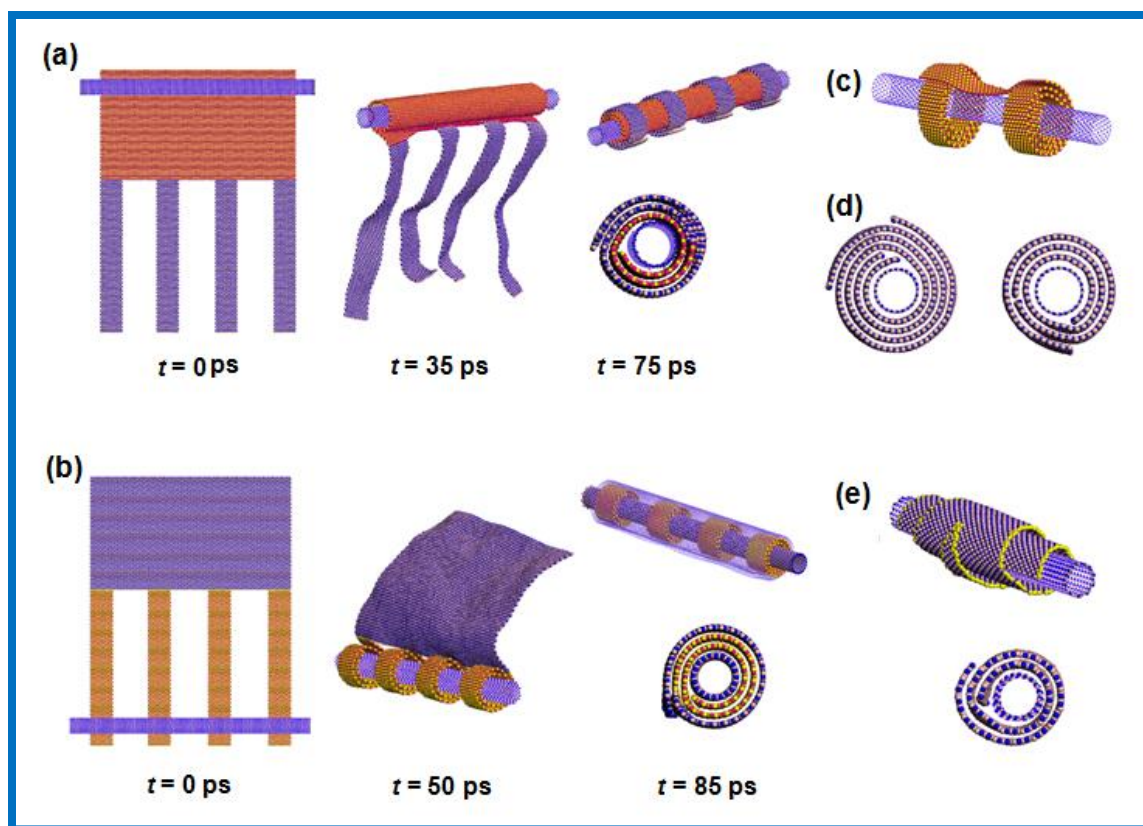


Fig. 7 The self-assembly of structured *h*-BN flakes on BNNTs. (a) Formation of *h*-BN scroll covered with four bilayered *h*-BN rings on the tube at different time. (b) Formation of the nanostructure with four bilayered *h*-BN rings covered by *h*-BN layers on the tube. (c) Dumbbell-like structure is formed on the BNNT. (d) Single- and double-layered scrolls can be formed when bilayered *h*-BN sheet assemble on the BNNT depend on the *h*-BN length. (e) A ladder scroll structure formed when a triangular *h*-BN wraps onto BNNT.

Considering that for lots of applications, *h*-BN nanostructures are required with more complex geometries along specific dimensions. Novel composite functional materials could be fabricated if *h*-BN with various shapes and sizes are self-assembled on the surfaces of nanoscale materials. It is interesting to explore the self-assembly

dynamics of a comb-like *h*-BN nanostructure with four *h*-BN nanoribbons on BNNT.¹³ One end of all four ribbons ($161.912 \times 22.140 \text{ \AA}^2$) is connected to the remaining part ($207.35 \times 115.753 \text{ \AA}^2$) of the *h*-BN sheet, and the distances between the adjacent ribbons are 40.07 \AA . The length of the BNNB is 250 \AA . Initially, the remaining part is placed aside BNNT with distance of 8.0 \AA , just as seen in Fig. 7a. As the simulation goes on, the remaining part continuously scrolls around BNNT, and at $t = 35 \text{ ps}$, the *h*-BN makes a multilayered scroll structure. Then, four *h*-BN ribbons continuously wrap onto multilayered scroll to form multilayered ring structures at $t = 75 \text{ ps}$, seen the side and top views. While when placing the tips of all four *h*-BN ribbons on the (20,0) BNNT, as shown in Fig. 7b, they fold around the tube and form bilayered ring structures on the BNNT at $t = 50 \text{ ps}$. The rest of the *h*-BN sheet also folds on the bilayered ring structures and eventually completely wraps around the *h*-BN ribbons at $t = 85 \text{ ps}$ (side and top views). Then, the BNNTs are removed from their cores of the two self-assembled complex nanostructures, and the remaining configuration is equilibrated. Upon removal, the diameters of the scrolls did not change obviously and the systems still retains the same sharp stabilized by the *h*-BN layers. This property is distinct to graphene that the nanostructure with ribbons inside and outside will expand and shrink obviously, respectively.

Then the *h*-BN is cut to the shape that composed by an *h*-BN ribbon ($84.87 \times 14.91 \text{ \AA}^2$) vertically connected to two *h*-BN ribbons ($277.67 \times 15.99 \text{ \AA}^2$) with the gap of (52.89 \AA). The BNNT (15, 0) with fixed ends is located at the tips of *h*-BN ribbons. After the nanosystem is released, the ribbons roll around the BNNT individually, and eventually make a dumbbell-like structure that two scrolls connected by an *h*-BN bridge, as shown

in Fig. 7c. The self-assembly of bilayered *h*-BN with width of 22.014 Å on BNNT (12, 12) is further investigated. Fig. 7d shows that when bilayered *h*-BN is long enough, it will roll onto the BNNT like monolayered *h*-BN to form bilayered scroll. While if bilayered *h*-BN possesses relative shorter length, it will form single-layered scroll. However, due to the increase of rigidity with the increase of layer number, the BNNT can not induce the three-layered *h*-BN to self-assemble on it. The self-assembly of the *h*-BN nanostructure with triangular sharp on BNNT is also studied. The bottom length of triangle sheet is 173.27 Å and the highness is 332.1 Å. The BNNT is placed aside *h*-BN bottom. Fig. 7e shows that the triangular *h*-BN wrapping onto the BNNT and forms a ladder scroll structure after $t = 100$ ps. When placing the triangle tip aside the BNNT, the formation of ladder scroll will much be more difficult. It can also activate *h*-BN with trapezoid and other complex shapes to self-assemble on BNNT to produce complicated nanosystems. These results indicate that various structured *h*-BNs can be induced to scroll onto the BNNT and form various composite materials according to individual requirement.

4. Conclusion

This study provides a direct observation of the self-assembly of *h*-BN nanostructures onto BNNTs on an atomic scale. When $W \leq 9.232$ Å, thin *h*-BN ribbon can only form helix; while if W larger than the threshold of 17.753 Å, relative wider *h*-BN sheet can only form scroll on BNNT surface. It is worth noting when $9.232 < W < 17.753$ Å, *h*-BN self-assembles on BNNTs leading to a mechanically bistable configurations, helix and scroll. The size of BNNTs should meet the required conditions to guarantee the self-assemble. This unique phenomenon is the result of the combined action of the vdW interaction of *h*-BN and BNNT and that between *h*-BN layers, as well as the π - π stacking

effect, which stabilizes the adjacent paralleled *h*-BN layers to achieve the lowest energy AB stack. The vdW binding energy between *h*-BN sheet and BNNT increases with the increase of BNNT diameters. The *h*-BNs with arbitrary sizes and shapes can wrap onto BNNTs to form various configurations depending slightly on the tube chirality. The self-assembly conditions and the stability of the formed nanoconfigurations are investigated for numerous potential applications.

The proposed discoveries are crucial for deeper understanding of the graphene-like two-dimensional materials, which provides a powerful way to fabricate nanoscale composite functional materials and devices and tune their properties. These findings will further provide theoretical directions on the synthesis of *h*-BN-based composite nanomaterials and eventually on their applications. Perhaps, multifarious controllable configurations of structured *h*-BNs wrapped on BNNT suggests novel ways of improving the properties of BNNT, such as the electronic band gap and the concentration of charge carriers, which will pave the way for the progress of nanoelectronics.

Acknowledgments

This work was supported by the National Natural Science Foundation of China (Grant No. 51302126), the Natural Science Foundation of Shandong Province, China (Nos. ZR2013EMM001 and ZR2013AL008) and the Startup Foundation for Doctoral Research of Linyi University, Shandong Province, China (No. LYDX2013BS004).

References

- 1 K. S. Novoselov, A. K. Geim, S. V. Morozov, D. Jiang, Y. Zhang, S. V. Dubonos, I. V. Grigorieva and A. A. Firsov, *Science*, 2004, **306**, 666–669.
- 2 K. Novoselov, A. Geim, S. Morozov, D. Jiang, M. Katsnelson, I. Grigorieva, S. Dubonos, A. Firsov, *Nature*, 2005, **438**, 197–200.
- 3 M. S. Xu, D. Fujita, H. Z. Chen, N. Hanagata, *Nanoscale*, 2011, **3**, 2854–2858.
- 4 N. Ooi, A. Rairkar, L. Lindsley, J. B. Adams, *J. Phys. Condens. Matter.*, 2006, **18**, 97–115.
- 5 S. B. Tang, J. P. Yu, L. X. Liu, *Phys. Chem. Chem. Phys.*, 2013, **15**, 5067–5077.
- 6 J. Furthmüller, J. Hafner, G. Kresse, *Phys. Rev. B*, 1994, **50**, 15606–15622.
- 7 Y. Zhao, X. J. Wu, J. L. Yang, X. C. Zeng, *Phys. Chem. Chem. Phys.*, 2012, **14**, 5545–5550.
- 8 W. Schmolla, H. L. Hartnagel, *J. Phys. D: Appl. Phys.*, 1982, **15**, L95.
- 9 M. J. Rand, J. F. Roberts, *J. Electrochem. Soc.*, 1968, **115**, 423–429.
- 10 K. Miyoshi, D. H. Buckley, J. J. Pouch, S. A. Alterovitz, H. E. Sliney, *Surf. Coat. Technol.*, 1987, **33**, 221–233.
- 11 A. Lyalin, A. Nakayama, K. Uosaki, T. Taketsugu, *Phys. Chem. Chem. Phys.*, 2013, **15**, 2809–2820.
- 12 Y. F. Li, H. Q. Yu, H. Li, C. G. An, K. Zhang, K. M. Liew, X. F. Liu, *J. Phys. Chem. C*, 2009, **115**, 6229–6234.
- 13 N. Patra, Y. B. Song, P. Kral, *ACS Nano*, 2011, **5**, 1798–1804.
- 14 D. Xia, Q. Z. Xue, J. Xie, H. J. Chen, C. Lv, F. Besenbacher, M. D. Dong, *Small*, 2010, **6**, 2010–2019.

- 15 N. Patra, B. Y. Wang, P. Kral, *Nano Lett.*, 2009, **9**, 3766–3771.
- 16 L. M. Viculis, J. J. Mack, R. B. Kaner, *Science*, 2003, **299**, 1361.
- 17 D. Yu, F. Liu, *Nano Lett.*, 2007, **7**, 3046–3050.
- 18 A. Buldum, J. P. Lu, *Phys. Rev. Lett.*, 1999, **83**, 5050–5053.
- 19 L. Ortolani, F. Houdellier, M. Monthieux, V. Morandi, *Carbon*, 2010, **48**, 3050–3056.
- 20 A. K. Rappé, C. J. Casewit, K. S. Colwell, W. A. Goddard, W. M. Skiff, *J. Am. Chem. Soc.*, 1992, **114**, 10024–10035.
- 21 C. J. Casewit, K. S. Colwell, A. K. Rappé, *J. Am. Chem. Soc.* 1992, **114**, 10035–10046; 1992, **114**, 10046–10053.
- 22 D. H. Jung, D. Kim, T. B. Lee, S. B. Choi, J. H. Yoon, J. Kim, K. Choi, S. H. Choi, *J. Phys. Chem. B*, 2006, **110**, 22987–22990.
- 23 Y. K. Zhou, S. Adams, R. P. Rao, D. D. Edwards, A. Neiman, N. Pestereva, *Chem. Mater.*, 2008, **20**, 6335–6345.
- 24 M. L. Głóbwka, D. Martynowski, K. Kozłowska, *J. Mol. Struct.*, 1999, **474**, 81–89.
- 25 C. A. Hunter, J. K. M. Sanders, *J. Am. Chem. Soc.*, 2009, **112**, 5525–5534.
- 26 E. A. Gazit, *FASEB J.*, 2002, **16**, 77–83.
- 27 Q. B. Zheng, Q. Z. Xue, K. Y. Yan, L. Z. Hao, Q. Li, X. L. Gao, *J. Phys. Chem. C*, 2007, **111**, 4628–4635.
- 28 Q. Lu, M. Arroyo, R. Huang, *J. Phys. D: Appl. Phys.*, 2009, **42**, 102002–102007.
- 29 J. Atalaya, A. Isacson, J. M. Kinaret, *Nano Lett.*, 2008, **8**, 4196–4200.